Check for updates

IET Radar, Sonar & Navigation

WILEY

The Institution of Engineering and Technology

ORIGINAL RESEARCH OPEN ACCESS

MIMO Radar Detection Algorithms With Location Capabilities for Heterogeneous Environments

Tianqi Wang[1] | Chaoran Yin[1] | Da Xu[1] | Chengpeng Hao[1] | Danilo Orlando[2] | Giuseppe Ricci[3]

[1]Institute of Acoustics, Chinese Academy of Sciences, Beijing, China | [2]Dipartimento di Ingegneria dell'Informazione, Università di Pisa, Pisa, Italy | [3]Dipartimento di Ingegneria dell'Innovazione, Università del Salento, Lecce, Italy

Correspondence: Danilo Orlando (danilo.orlando@unipi.it)

Received: 4 August 2025 | **Revised:** 7 January 2026 | **Accepted:** 12 February 2026

Keywords: adaptive detection | covariance estimation | generalized likelihood ratio test | heterogeneous environments | MIMO radar | target localization

ABSTRACT

In this paper, we address the problem of joint adaptive detection and range-Doppler estimation for MIMO radar systems in heterogeneous environments. Specifically, we extend the Two-Step Generalised Likelihood Ratio Test Detector designed for homogeneous Gaussian background to work in compound-Gaussian scenarios. To this end, we replace the conventional sample covariance matrix of the secondary data with the estimators of clutter statistics based on the normalised sample covariance matrix and the recursive estimate. In this context, three detectors are proposed that can inherently provide estimates of target position in the delay-Doppler domain. Numerical examples demonstrate that the proposed detectors significantly outperform the homogeneous counterparts in heterogeneous environments whilst maintaining satisfying performance in homogeneous environments. Remarkably, the analysis of the false alarm rate reveals that the proposed detectors are insensitive to changes in the scaling factor and/or covariance structure of the background.

1 | Introduction

Nowadays, technological innovations have facilitated the development of new generations of radar systems that offer enhanced design flexibility for performance optimisation. In this context, colocated Multiple-Input Multiple-Output (MIMO) radar systems have emerged as a sophisticated extension of the standard phased-array radars that belong to the category of Single-Input Multiple-Output (SIMO) systems [1, 2]. Unlike traditional SIMO systems, MIMO radars transmit multiple waveforms that can exhibit a certain correlation gradation (achieving waveform diversity). In [3], the authors present a comprehensive review of the advantages of colocated MIMO radars in terms of system performance (i.e., detection, estimation, beamforming, etc.). As for target detection, which can be defined as the main function of a radar system, in [4–11] many important architectures based upon MIMO radars are developed. We refer the readers to these literature for technical details and in-depth analysis.

Literature on adaptive detection for MIMO radars predominantly uses a signal model that assumes a matched filter perfectly tuned to a specific delay-Doppler (or range-Doppler) bin. Otherwise stated, the scatterer representing a point-like target is located exactly in the centre of the considered bin, thereby disregarding the actual energy distribution across the range-Doppler domain [12, 13]. As a consequence, the so-called 'straddle loss' [14], (Ch. 14 and 18) occurs due to the 'asynchronous sampling' of the delay-Doppler domain. It is important to notice that this aspect is also valid for phased arrays as corroborated by work in [15]. Indeed, it develops a more accurate signal model taking into account the target energy spillover over the range bins. Based on this discrete-time model, detection architectures with target position estimation capabilities are proposed for the first time. Specifically, by capitalising the energy spreading over multiple range bins, this kind of architectures can outperform the conventional approaches while simultaneously providing a rough target position estimate within the range bin under test. Such information can be used to enhance the tracking stage performance of the system.

This is an open access article under the terms of the Creative Commons Attribution License, which permits use, distribution and reproduction in any medium, provided the original work is properly cited.

© 2026 The Author(s). *IET Radar, Sonar & Navigation* published by John Wiley & Sons Ltd on behalf of The Institution of Engineering and Technology.

Inspired by the work of [15] and further developments [16–19], in [20], the authors use a more accurate MIMO radar signal model that accounts for the energy spillover over the delay-Doppler domain and formulate a binary hypothesis test that encompasses all the possible energy configurations. By applying the Generalised Likelihood Ratio Test (GLRT) [21] along with the two-step modification [22] when possible or ad hoc approximations of it, three detection architectures are derived for MIMO radars. A thorough performance analysis of the proposed architectures is presented in [23, 24], where they are proved to possess the Constant False Alarm Rate (CFAR) property with respect to the power of the disturbance. In addition, simulations show that they are substantially insensitive to structure mismatches of the clutter covariance matrix under several operating scenarios. Moreover, these architectures are more robust than competitors introduced by [20] to target steering vector mismatches.

Actually, the detection architectures developed in [20] rely on the common design assumptions of homogeneous Gaussian distributed clutter. However, as confirmed by the experimental measurements [25–27], the above assumptions are not always effective. For example, in real high-resolution radar systems, particularly at low grazing angles, clutter is better modelled as a compound Gaussian process whose complex envelope is given by the product of a speckle component and a texture component. In more detail, the speckle component follows the (circularly-symmetric) complex Gaussian distribution and the texture component is a real, nonnegative and slowly varying random process [28, 29]. Under sufficiently short time observation intervals, the compound Gaussian process degrades into a spherically invariant random process and the texture component can be approximated as a random constant [28, 29]. In this scenario, each range bin in the surveillance area of the radar is characterised by a specific texture whose value may vary along the range [30]. The literature on target detection in nonhomogeneous environments is densely populated (see, for instance, [31–34]). In [33], the Normalised Sample Covariance Matrix (NSCM) is exploited to design an adaptive detection algorithm that is CFAR with respect to the texture statistics. In [34], a detector using a Recursive Estimation of the Covariance Matrix (RECM) is derived for the case of heterogeneous Gaussian disturbance, which possesses CFAR property with respect to the unknown statistics of the disturbance under a suitable initialisation.

With the above remarks in mind and in the context of MIMO radars, we extend the joint detection and delay-Doppler estimation problem considered in [20] to a more realistic heterogeneous environment. As a matter of fact, the detection architectures proposed in [20] are developed and assessed under homogeneous clutter. Although this assumption is reasonable for the detector design since it allows for mathematical tractability, in practice it can give rise to critical issues such as an increased number of false alarms or a detection performance degradation. For this reason, we use the so-called two-step GLRT design criterion [22] and, unlike [20] where the plain sample covariance matrix is used, we couple the obtained decision scheme with the NSCM and the RECM to come up with three new detectors for MIMO radars capable of working in heterogeneous scenarios. Such a design choice would allow for a better control of the false alarms because these covariance estimates account for clutter power variations, whereas the plain sample covariance matrix used in [20] no longer represents a reliable estimator of the clutter statistical properties in nonhomogeneous conditions. At the analysis stage, we assess the performance of the newly proposed algorithms focusing on three aspects, that is, CFAR property, detection performance and estimation performance (for target location).

The remainder of this paper is organised as follows. Section 2 contains the problem formulation and Section 3 is devoted to the design of the detectors for heterogeneous clutter-dominated environments. Section 4 provides numerical examples and comparisons. Concluding remarks are given in Section 5.

1.1 | Notation

Vectors (matrices) are denoted by boldface lower- (upper-) case letters. $\det(\cdot)$, $\mathrm{Tr}(\cdot)$, $(\cdot)^*$, $(\cdot)^T$ and $(\cdot)^\dagger$ denote the determinant, the trace, complex conjugate, transpose and complex conjugate transpose, respectively. If A and B are two generic sets, $A \times B$ denotes the Cartesian product, whereas $A\backslash B$ denotes the difference set. $\mathbb{C}$ ($\mathbb{N}$) is the set of complex (natural) numbers, whereas $\mathbb{C}^{N\times M}$ is the Euclidean space of $(N \times M)$-dimensional complex matrices; the set of real numbers is denoted by $\mathbb{R}$. $\boldsymbol{I}$ and $\boldsymbol{0}$ stand for the identity matrix and the null matrix of suitable sizes, respectively. $\otimes$ is the Kronecker product and $|\cdot|$ is the modulus of a scalar. $\boldsymbol{x} \sim \mathcal{CN}_N(\boldsymbol{\mu}, \boldsymbol{R})$ means that $\boldsymbol{x}$ is a complex circular N-dimensional normal vector with mean $\boldsymbol{\mu}$ and covariance matrix $\boldsymbol{R}$.

2 | Problem Formulation

Let us consider a colocated MIMO radar employing N_t antennas on transmit and N_r antennas on receive. Assuming that the values of the Ambiguity Function (AF) are negligible outside a rectangular region of width $\Delta\tau_{ML}$ along the delay dimension and Δf_{ML} along the Doppler dimension, the delay-Doppler region of interest is sampled at $\Delta\tau_s = \Delta\tau_{ML}/2$ and $\Delta f_s = \Delta f_{ML}/2$ to obtain delay-Doppler bins of size $\Delta\tau_s \times \Delta f_s$. When a point-like target from a given direction θ_t appears in the delay-Doppler bin centred at $\tau_l = l\Delta\tau_s$ and $f_{d,h} = h\Delta f_s$, $l, h \in \mathbb{N}$ $(l, h \geq 2)$, the corresponding vector of echoes can be written as [35].

$$\boldsymbol{z}_{l,h} = \alpha_t\left[\boldsymbol{I}\otimes\boldsymbol{C}\left(\Delta\tau_l, \Delta f_{d,h}\right)\right]\boldsymbol{v}(\theta_t) + \boldsymbol{w}_{l,h} \in \mathbb{C}^{N\times 1}, \tag{1}$$

where $\alpha_t \in \mathbb{C}$ is an unknown deterministic factor representative of channel and target responses, $\boldsymbol{I}$ has size $N_R \times N_R$, $\boldsymbol{C}\left(\Delta\tau_l, \Delta f_{d,h}\right) \in \mathbb{C}^{N_T\times N_T}$ is the vector AF of the transmitted signal $\boldsymbol{s}(t) \in \mathbb{C}^{N_T\times 1}$, which is expressed as [13, 35].

$$\boldsymbol{C}\left(\Delta\tau_l, \Delta f_{d,h}\right) = \int_0^{T_p} \boldsymbol{s}(t - \Delta\tau_l)^* \boldsymbol{s}(t)^T e^{-j2\pi\Delta f_{d,h} t} dt, \tag{2}$$

T_p is the pulse duration, $\Delta\tau_l = \tau_l - \tau_t$, $\Delta f_{d,h} = f_{d,h} - f_{d,t}$ with $(\tau_t, f_{d,t})$ the unknown coordinates of the target in the delay-Doppler domain, $\boldsymbol{v}(\theta) \in \mathbb{C}^{N\times 1}$ is the virtual array manifold

17518792, 2026, 1, Downloaded from https://ietresearch.onlinelibrary.wiley.com/doi/10.1049/rsn2.70127 by CochraneItalia, Wiley Online Library on [29/04/2026]. See the Terms and Conditions (https://onlinelibrary.wiley.com/terms-and-conditions) on Wiley Online Library for rules of use; OA articles are governed by the applicable Creative Commons License

with $N = N_T N_R$ and θ_t the target angle of arrival, whereas $\boldsymbol{w}_{l,h} \in \mathbb{C}^{N\times 1}$ is the interference component.

As illustrated in Figure 1, to detect the possible target, we need to consider all the likely positions of the target within the delay-Doppler bin. Specifically, the entries of the vector ambiguity function become negligible outside a rectangular region of the delay-Doppler domain. As a consequence, according to the grid generated by the time and Doppler sampling, the positions of this region depend on the actual values of the target delay and Doppler that generate a relative displacement with respect to the points of the grid. Therefore, we process echoes from a 3 × 3 window containing the delay-Doppler samples indexed by

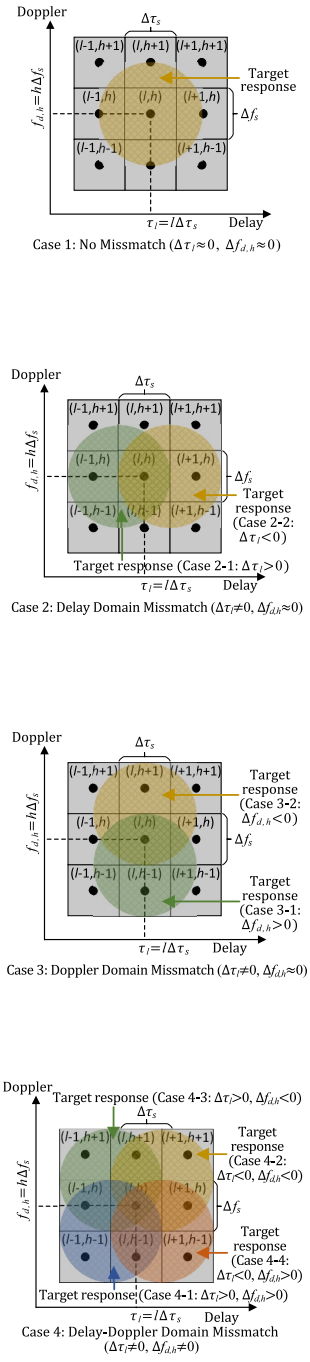

FIGURE 1 | Target positions within the delay-Doppler domain.

$\Omega_{l,h} = \{l-1, l, l+1\} \times \{h-1, h, h+1\}$, where l and h are the index values minimising $|\Delta\tau_l|$ and $|\Delta f_{d,h}|$, respectively. Four cases are considered in Figure 1 according to the actual values of $\Delta\tau_l$ and $\Delta f_{d,h}$. In the first case, the target response is almost entirely contained in the delay-Doppler bin under test indexed by (l, h) whereas the samples in the surrounding bins contain negligible target components. In the other three cases, a significant mismatch with respect to the delay and/or Doppler occurs. In such cases, the surrounding bins contain target components that can be exploited to integrate target energy and improve the detection performance. According to each target configuration within $\Omega_{l,h}$ (all the possible situations are listed by Equations (3–11) in [20] and are omitted here for brevity), we can define a subset $\Omega_t \subset \Omega_{l,h}$ that indexes the samples contaminated by target components.For instance, if Equation (5) of [20] holds, $\Omega_t = \{(l, h), (l+1, h)\}$. Notice that Ω_t is unknown.

Thus, the problem of detecting a possible target located in the delay-Doppler bin indexed by (l, h) can be formulated as a binary hypothesis test where the alternative hypothesis accounts for the possible situations listed by Equations (3–11) in [20], namely

$$\begin{cases} H_0: \begin{cases} \boldsymbol{z}_{n,m} = \boldsymbol{w}_{n,m}, & (n,m) \in \Omega_{l,h}, \\ \boldsymbol{r}_k = \boldsymbol{w}_k, & k = 1, \cdots, K_S, \end{cases} \\ H_1: \begin{cases} \boldsymbol{z}_{n,m} = \alpha_t \boldsymbol{p}_{n-l,m-h} + \boldsymbol{w}_{n,m}, & (n,m) \in \Omega_t, \\ \boldsymbol{z}_{n,m} = \boldsymbol{w}_{n,m}, & (n,m) \in \Omega_{l,h} \backslash \Omega_t, \\ \boldsymbol{r}_k = \boldsymbol{w}_k, & k = 1, \cdots, K_S, \end{cases} \end{cases} \tag{3}$$

where $\boldsymbol{r}_k$, $k = 1, ..., K_S$, are secondary data vectors which are statistically independent of each other and of the echo vectors in the Window Under Test (WUT), $\boldsymbol{p}_{n-l,m-h} = \boldsymbol{A}_{n-l,m-h}\boldsymbol{v}(\theta_t) \in \mathbb{C}^{N\times 1}$, $\boldsymbol{A}_{n-l,m-h} = \boldsymbol{I} \otimes \boldsymbol{C}(\Delta\tau_n, \Delta f_{d,m}) \in \mathbb{C}^{N\times N}$, the $\boldsymbol{w}_{n,m}$s and $\boldsymbol{w}_k$s are statistically independent interference components modelled as follows

$$\boldsymbol{w}_{n,m} = \gamma_{n,m}\boldsymbol{g}_{n,m}, \ (n,m) \in \Omega_{l,h}, \tag{4}$$

$$\boldsymbol{w}_k = \gamma_k \boldsymbol{g}_k, \ k = 1, ..., K_S, \tag{5}$$

where $\boldsymbol{g}_{n,m}$, $\boldsymbol{g}_k \sim \mathcal{CN}_N(\boldsymbol{0}, \boldsymbol{\Sigma})$ with $\boldsymbol{\Sigma}$ the positive definite covariance matrix, the $\gamma_{n,m}$s and γ_ks are positive scaling factors representative of the interference power. When $\gamma_{n,m} = \gamma_k = \gamma > 0$, $(n, m) \in \Omega_{l,h}$ and $k = 1, ..., K_S$, the background interference reduces to the homogeneous environment and we have

$$\boldsymbol{w}_{n,m}, \ \boldsymbol{w}_k \sim \mathcal{CN}_N(\boldsymbol{0}, \boldsymbol{M}), \ (n,m) \in \Omega_{l,h}, \quad k = 1, ..., K_S, \tag{6}$$

with $\boldsymbol{M} = \gamma^2\boldsymbol{\Sigma}$ the covariance matrix.

3 | Detector Designs

In this section, we design the detectors resorting to the two-step GLRT-based criterion. The first step of this design procedure assumes that the Background Interference Covariance Matrix (BICM) is known and computes the GLRT by considering the vectors in the WUT. To be more definite, the GLRT for known BICM has the following expression

17518792, 2026, 1, Downloaded from https://ietresearch.onlinelibrary.wiley.com/doi/10.1049/rsn2.70127 by CochraneItalia, Wiley Online Library on [29/04/2026]. See the Terms and Conditions (https://onlinelibrary.wiley.com/terms-and-conditions) on Wiley Online Library for rules of use; OA articles are governed by the applicable Creative Commons License

$$\max_{\Delta\tau_l,\Delta f_{d,h}} \max_{\alpha_t} \frac{\prod_{(n,m)\in\Omega_{l,h}} f_1\left(\boldsymbol{z}_{n,m};i_{n,m}\alpha_t, i_{n,m}\Delta\tau_l, i_{n,m}\Delta f_{d,h}, \boldsymbol{M}_{n,m}\right)}{\prod_{(n,m)\in\Omega_{l,h}} f_0\left(\boldsymbol{z}_{n,m};\boldsymbol{M}_{n,m}\right)} \underset{H_0}{\overset{H_1}{\gtrless}} \eta, \quad (7)$$

where $\boldsymbol{M}_{n,m} = \gamma_{n,m}^2\boldsymbol{\Sigma}$, $i_{n,m} = 1$ if $(n,m) \in \Omega_t$ and $i_{n,m} = 0$ otherwise, η is the detection threshold that allows for the control of the Probability of False Alarm (P_{fa}), $f_1\left(\boldsymbol{z}_{n,m};i_{n,m}\alpha_t, i_{n,m}\Delta\tau_l, i_{n,m}\Delta f_{d,h}, \boldsymbol{M}_{n,m}\right)$ is the Probability Density Function (PDF) of $\boldsymbol{z}_{n,m}$ under H_1 with expression

$$\begin{aligned} &f_1\left(\boldsymbol{z}_{n,m};i_{n,m}\alpha_t, i_{n,m}\Delta\tau_l, i_{n,m}\Delta f_{d,h}, \boldsymbol{M}_{n,m}\right) \\ &= \frac{\exp\left\{-\operatorname{Tr}\left[\boldsymbol{M}_{n,m}^{-1}(\boldsymbol{z}_{n,m} - i_{n,m}\alpha_t\boldsymbol{p}_{n-l,m-h})(\boldsymbol{z}_{n,m} - i_{n,m}\alpha_t\boldsymbol{p}_{n-l,m-h})^\dagger\right]\right\}}{\pi^N\det(\boldsymbol{M}_{n,m})}, \end{aligned} \quad (8)$$

and $f_0\left(\boldsymbol{z}_{n,m};\boldsymbol{M}_{n,m}\right)$ is the PDF of $\boldsymbol{z}_{n,m}$ under H_0 given by

$$f_0\left(\boldsymbol{z}_{n,m};\boldsymbol{M}_{n,m}\right) = \frac{\exp\left\{-\operatorname{Tr}\left[\boldsymbol{M}_{n,m}^{-1}\boldsymbol{z}_{n,m}\boldsymbol{z}_{n,m}^\dagger\right]\right\}}{\pi^N\det(\boldsymbol{M}_{n,m})}. \quad (9)$$

Maximising the numerator of Equation (7) with respect to α_t is tantamount to

$$\min_{\alpha_t} \sum_{(n,m)\in\Omega_t} \left(\boldsymbol{z}_{n,m} - \alpha_t\boldsymbol{p}_{n-l,m-h}\right)^\dagger \boldsymbol{M}_{n,m}^{-1}\left(\boldsymbol{z}_{n,m} - \alpha_t\boldsymbol{p}_{n-l,m-h}\right) \quad (10)$$

whose solution is

$$\widehat{\alpha}_t = \frac{\sum_{(n,m)\in\Omega_t} \boldsymbol{p}_{n-l,m-h}^\dagger \boldsymbol{M}_{n,m}^{-1}\boldsymbol{z}_{n,m}}{\sum_{(n,m)\in\Omega_t} \boldsymbol{p}_{n-l,m-h}^\dagger \boldsymbol{M}_{n,m}^{-1}\boldsymbol{p}_{n-l,m-h}}. \quad (11)$$

Replacing the above result in Equation (7) and taking the logarithm, we obtain

$$\max_{\Delta\tau_l,\Delta f_{d,h}} \frac{\left|\sum_{(n,m)\in\Omega_t} \boldsymbol{p}_{n-l,m-h}^\dagger \boldsymbol{M}_{n,m}^{-1}\boldsymbol{z}_{n,m}\right|^2}{\sum_{(n,m)\in\Omega_t} \boldsymbol{p}_{n-l,m-h}^\dagger \boldsymbol{M}_{n,m}^{-1}\boldsymbol{p}_{n-l,m-h}} \underset{H_0}{\overset{H_1}{\gtrless}} \eta, \quad (12)$$

with η denoting a modification of the original threshold (see the Appendix A for a proof of the above results).Hereafter, we denote by η the generic detection threshold.

The second step of the design procedure consists in replacing the BICM with a suitable estimate based upon the secondary data. In what follows, we use the NSCM (along with a heuristic modification of it) and the RECM to obtain three new decision schemes for heterogeneous environments.

Finally, the maximisation with respect to the pair $(\Delta\tau_l, \Delta f_{d,h})$ is conducted over a 2-dimensional grid. Considering different degrees of requirements for accuracy and computational load, several sampling steps and search strategies can be pursued, which are described in Section 3-A5 of [20]. In this paper, the search grid is built up by the sets $\left\{\frac{n_\tau - N_\tau}{2N_\tau}\Delta\tau_s\right\}_{n_\tau=0}^{2N_\tau}$, $N_\tau \in \mathbb{N}$ for $\Delta\tau_l$ and $\left\{\frac{n_f - N_f}{2N_f}\Delta f_s\right\}_{n_f=0}^{2N_f}$, $N_f \in \mathbb{N}$ for $\Delta f_{d,h}$.

3.1 | Detector Using the Normalised Sample Covariance Matrix

The natural estimate for the structure of the BICM in the case where the clutter power varies with the range is represented by the NSCM given by [36].

$$\widehat{\boldsymbol{\Sigma}} = \frac{N}{K_S}\sum_{k=1}^{K_S} \frac{\boldsymbol{r}_k\boldsymbol{r}_k^\dagger}{\boldsymbol{r}_k^\dagger\boldsymbol{r}_k}. \quad (13)$$

As for the clutter power, an intuitive estimate can be obtained by averaging the square of the data vector components after whitening through the NSCM, namely

$$\widehat{\gamma}_{n,m}^2 = \frac{1}{N}\boldsymbol{z}_{n,m}^\dagger\widehat{\boldsymbol{\Sigma}}^{-1}\boldsymbol{z}_{n,m}. \quad (14)$$

Based on the above results, we obtain

$$\max_{\Delta\tau_l,\Delta f_{d,h}} \frac{\left|\sum_{(n,m)\in\Omega_t} \boldsymbol{p}_{n-l,m-h}^\dagger\left(\widehat{\gamma}_{n,m}^2\widehat{\boldsymbol{\Sigma}}\right)^{-1}\boldsymbol{z}_{n,m}\right|^2}{\sum_{(n,m)\in\Omega_t} \boldsymbol{p}_{n-l,m-h}^\dagger\left(\widehat{\gamma}_{n,m}^2\widehat{\boldsymbol{\Sigma}}\right)^{-1}\boldsymbol{p}_{n-l,m-h}} \underset{H_0}{\overset{H_1}{\gtrless}} \eta, \quad (15)$$

which is referred to in the following as the NSCM-based Two-Step GLRT Detector (NSCM-TS-GLRT-D).

3.2 | Detector Using the Recursive Estimation of the Covariance Matrix

Exploiting the recursive estimation procedure developed in [34], the RECM-based Two-Step GLRT Detector (RECM-TS-GLRT-D) can be written as

$$\max_{\Delta\tau_l,\Delta f_{d,h}} \frac{\left|\sum_{(n,m)\in\Omega_t} \boldsymbol{p}_{n-l,m-h}^\dagger\left(\tilde{\gamma}_{n,m}^2\tilde{\boldsymbol{\Sigma}}^{(i_{\max})}\right)^{-1}\boldsymbol{z}_{n,m}\right|^2}{\sum_{(n,m)\in\Omega_t} \boldsymbol{p}_{n-l,m-h}^\dagger\left(\tilde{\gamma}_{n,m}^2\tilde{\boldsymbol{\Sigma}}^{(i_{\max})}\right)^{-1}\boldsymbol{p}_{n-l,m-h}} \underset{H_0}{\overset{H_1}{\gtrless}} \eta, \quad (16)$$

where $i_{\max}$ is the maximum number of iterations for the following update rule

$$\tilde{\boldsymbol{\Sigma}}^{(i+1)} = \frac{N}{K_S}\sum_{k=1}^{K_S} \frac{\boldsymbol{r}_k\boldsymbol{r}_k^\dagger}{\boldsymbol{r}_k^\dagger\left(\tilde{\boldsymbol{\Sigma}}^{(i)}\right)^{-1}\boldsymbol{r}_k}, \quad (17)$$

with $\tilde{\boldsymbol{\Sigma}}^{(0)}$ being the NSCM, i the iteration index, and

$$\tilde{\gamma}_{n,m}^2 = \frac{1}{N}\boldsymbol{z}_{n,m}^\dagger\left(\tilde{\boldsymbol{\Sigma}}^{(i_{\max})}\right)^{-1}\boldsymbol{z}_{n,m}. \quad (18)$$

3.3 | Detector Using a Hybrid Estimation of the Covariance Matrix

In this last subsection, we propose a hybrid estimation of the BICM. Specifically, we couple the NSCM with the estimates of the scaling factors obtained through the recursive approach described

17518792, 2026, 1, Downloaded from https://ietresearch.onlinelibrary.wiley.com/doi/10.1049/rsn2.70127 by CochraneItalia, Wiley Online Library on [29/04/2026]. See the Terms and Conditions (https://onlinelibrary.wiley.com/terms-and-conditions) on Wiley Online Library for rules of use; OA articles are governed by the applicable Creative Commons License

in the previous subsection. Therefore, we use Equation (18) into Equation (15) in place of Equation (14) to come up with

$$\max_{\Delta\tau_l,\Delta f_{d,h}} \frac{\left|\sum_{(n,m)\in\Omega_t} \boldsymbol{p}_{n-l,m-h}^{\dagger}\left(\tilde{\gamma}_{n,m}^2\widehat{\boldsymbol{\Sigma}}\right)^{-1}\boldsymbol{z}_{n,m}\right|^2}{\sum_{(n,m)\in\Omega_t} \boldsymbol{p}_{n-l,m-h}^{\dagger}\left(\tilde{\gamma}_{n,m}^2\widehat{\boldsymbol{\Sigma}}\right)^{-1}\boldsymbol{p}_{n-l,m-h}} \underset{H_0}{\overset{H_1}{>\atop<}} \eta, \tag{19}$$

referred to as Heuristic Two-Step GLRT Detector (H-TS-GLRT-D).

4 | Illustrative Examples and Discussion

Before starting the performance analysis in both homogeneous and heterogeneous environments, we describe the considered competitors. Specifically, the first term of comparison is the Two-Step GLRT Detector (TS-GLRT-D) proposed in [20] for the homogeneous environment. This detector uses the plain Sample Covariance Matrix (SCM)

$$\widehat{\boldsymbol{M}} = \frac{1}{K_S}\sum_{k=1}^{K_S}\boldsymbol{r}_k\boldsymbol{r}_k^{\dagger} \tag{20}$$

and its expression is (for further details, we refer the reader to [20])

$$\max_{\Delta\tau_l,\Delta f_{d,h}} \frac{\left|\sum_{(n,m)\in\Omega_t} \boldsymbol{p}_{n-l,m-h}^{\dagger}\widehat{\boldsymbol{M}}^{-1}\boldsymbol{z}_{n,m}\right|^2}{\sum_{(n,m)\in\Omega_t} \boldsymbol{p}_{n-l,m-h}^{\dagger}\widehat{\boldsymbol{M}}^{-1}\boldsymbol{p}_{n-l,m-h}} \underset{H_0}{\overset{H_1}{>\atop<}} \eta. \tag{21}$$

The other competitors share a common basis, namely the GLRT for known $\boldsymbol{M}_{n,m}$ that assumes the presence of independent target components, represented by $\alpha_{n,m}\boldsymbol{p} = \alpha_{n,m}[\boldsymbol{I}\otimes\boldsymbol{C}(0,0)]\boldsymbol{v}(\theta_t)$, in each delay-Doppler bin indexed by $\Omega_{l,h}$. The related decision statistic is given by [37].

$$\sum_{(n,m)\in\Omega_{l,h}} \frac{\left|\boldsymbol{p}^{\dagger}\boldsymbol{M}_{n,m}^{-1}\boldsymbol{z}_{n,m}\right|^2}{\boldsymbol{p}^{\dagger}\boldsymbol{M}_{n,m}^{-1}\boldsymbol{p}} \underset{H_0}{\overset{H_1}{>\atop<}} \eta. \tag{22}$$

Now, the Conventional Two-Step GLRT (C-TS-GLRT) is obtained by replacing $\boldsymbol{M}_{n,m}$ with $\widehat{\boldsymbol{M}}$. The remaining competitors can be derived by using $\hat{\gamma}_{n,m}^2\widehat{\boldsymbol{\Sigma}}$, $\tilde{\gamma}_{n,m}^2\tilde{\boldsymbol{\Sigma}}^{(i_{\max})}$ and $\tilde{\gamma}_{n,m}^2\widehat{\boldsymbol{\Sigma}}$ in place of $\boldsymbol{M}_{n,m}$ to obtain the NSCM-based Conventional Two-Step GLRT (NSCM-C-TS-GLRT), the RECM-based Conventional Two-Step GLRT (RECM-C-TS-GLRT) and the Heuristic Conventional Two-Step GLRT (H-C-TS-GLRT), respectively.

The performance assessment is conducted under both homogeneous environment and heterogeneous environment. Specifically, we consider the following performance metrics: the actual P_{fa} (denoted by $\widehat{P}_{\text{fa}}$), the Probability of detection (P_{d}) and the Root Mean Square (RMS) estimation errors for $\Delta\tau_l$ and $\Delta f_{d,h}$. These metrics are estimated by means of the standard Monte Carlo counting techniques: as for the $\widehat{P}_{\text{fa}}$ and detection thresholds, they are computed over $100/P_{\text{fa}}$ independent trials with a nominal $P_{\text{fa}} = 10^{-3}$; the P_{d} (along with the RMS estimation errors) are computed over $N_{\text{Trial}} = 10^3$ independent trials. The RMS estimation errors for $\Delta\tau_l$ and $\Delta f_{d,h}$ are computed by using

$$\delta_{\text{rms},\Delta\tau_l} = \sqrt{\frac{1}{N_{\text{Trial}}}\sum_{n_T=1}^{N_{\text{Trial}}}\left|\Delta\widehat{\tau}_{l,n_T} - \Delta\tau_{l,n_T}^{t}\right|^2}, \tag{23}$$

$$\delta_{\text{rms},\Delta f_{d,h}} = \sqrt{\frac{1}{N_{\text{Trial}}}\sum_{n_T=1}^{N_{\text{Trial}}}\left|\Delta\widehat{f}_{d,h,n_T} - \Delta f_{d,h,n_T}^{t}\right|^2}, \tag{24}$$

with $\Delta\tau_{l,n_T}^{t}\left(\Delta f_{d,h,n_T}^{t}\right)$ the actual value for $\Delta\tau_l\left(\Delta f_{d,h}\right)$ generated in the n_Tth trial and $\Delta\widehat{\tau}_{l,n_T}\left(\Delta\widehat{f}_{d,h,n_T}\right)$ the estimate of $\Delta\tau_l\left(\Delta f_{d,h}\right)$ obtained at the n_Tth trial. For brevity, we only consider the most complex situation where the spillover of target energy involves both delay and Doppler dimensions. For this situation, the actual value of $\Delta\tau_l$ and $\Delta f_{d,h}$ ($\Delta\tau_l^t$ and $\Delta f_{d,h}^t$ say) are generated (independently from trial to trial and) uniformly distributed in $[-\Delta\tau_s/2, \Delta\tau_s/2]$ and $\left[-\Delta f_s/2, \Delta f_s/2\right]$, respectively.

Under the homogeneous assumption, in addition to the clutter, a small thermal noise component is also considered as part of the background interference and the definition of Signal to Clutter plus Noise Ratio (SCNR) is given by $\text{SCNR} = |\alpha_t|^2\boldsymbol{p}^{\dagger}\boldsymbol{M}^{-1}\boldsymbol{p}$, where $\boldsymbol{M} = \sigma_n^2\boldsymbol{I} + \boldsymbol{M}_c$ with $\sigma_n^2 = 1$ the noise power and $\boldsymbol{M}_c$ the clutter covariance matrix. The (n_1, n_2)th entry of $\boldsymbol{M}_c$ is $\sigma_c^2\rho^{|n_1-n_2|}$, $n_1, n_2 = 1, ..., N$, where σ_c^2 is set according to the Clutter to Noise Ratio (CNR) defined as $\text{CNR} = \sigma_c^2/\sigma_n^2$ and ρ is the one-lag correlation coefficient.

While under the heterogeneous environment, the interference vectors obey the compound Gaussian distribution, namely

$$\boldsymbol{w}_{n,m} = \sqrt{s_{n,m}}\boldsymbol{g}_{n,m},\ (n,m)\in\Omega_{l,h} \tag{25}$$

$$\boldsymbol{w}_k = \sqrt{s_k}\boldsymbol{g}_k,\ k = 1, ..., K_S, \tag{26}$$

where the $\boldsymbol{g}_{n,m}, \boldsymbol{g}_k$s are the speckle components such that $\boldsymbol{g}_{n,m}, \boldsymbol{g}_k \sim \mathcal{CN}_N(\boldsymbol{0}, \boldsymbol{\Sigma}_0)$ with $\boldsymbol{\Sigma}_0$ the positive definite covariance matrix, the $\sqrt{s_{n,m}}$s and $\sqrt{s_k}$s are the texture components statistically independent of the speckle and distributed as the square root of Gamma random variables with parameters $(\nu, 1/\nu)$ (so that the mean square value is unitary). The (n_1, n_2)th entry of $\boldsymbol{\Sigma}_0$ is $\rho^{|n_1-n_2|}$, $n_1, n_2 = 1, ..., N$, with ρ the one-lag correlation coefficient. Under the above assumptions, the Signal to Clutter Ratio (SCR) is defined as $\text{SCR} = |\alpha_t|^2\boldsymbol{p}^{\dagger}\boldsymbol{\Sigma}_0^{-1}\boldsymbol{p}$.

All the illustrative examples assume that $N_T = N_R = 8$, $K_S = 128, \Delta\tau_s = 0.1\ \mu\text{s}, \Delta f_s = 150\ \text{kHz}$ and $N_\tau = N_f = 5$. The generation of the waveform vector $\boldsymbol{s}(t)$ and the vector AF $\boldsymbol{C}\left(\Delta\tau_l, \Delta f_{d,h}\right)$ are described in Section 3 of supplementary material associated with [20], where the code length, N_c say, is set to 64. The virtual array manifold is given by $\boldsymbol{v}(\theta_t) = \boldsymbol{v}_R(\theta_t)\otimes\boldsymbol{v}_T(\theta_t)$ with $\boldsymbol{v}_R(\theta_t) = \left[1, e^{j\pi\sin\theta_t}, ..., e^{j\pi(N_R-1)\sin\theta_t}\right]^T/\sqrt{N_R}$, $\boldsymbol{v}_T(\theta_t) = \left[1, e^{j\pi\sin\theta_t}, ..., e^{j\pi(N_T-1)\sin\theta_t}\right]^T/\sqrt{N_T}$ and $\theta_t = 5°$.

17518792, 2026, 1, Downloaded from https://ietresearch.onlinelibrary.wiley.com/doi/10.1049/rsn2.70127 by CochraneItalia, Wiley Online Library on [29/04/2026]. See the Terms and Conditions (https://onlinelibrary.wiley.com/terms-and-conditions) on Wiley Online Library for rules of use; OA articles are governed by the applicable Creative Commons License

4.1 | Preliminary Step: Convergence Analysis of Equation (17)

As a preliminary step, we investigate the convergence rate of the recursive estimation procedure given by Equation (17). To this end, we consider the relative variation of the compressed log-likelihood function under H_1 at the ith iteration given by

$$\mathcal{L}_1^{(i)} = \max_{\Delta\tau_l, \Delta f_{d,h}} \log \prod_{(n,m)\in\Omega_{l,h}} f_1\Big(\boldsymbol{z}_{n,m}; i_{n,m}\widehat{\alpha}_t, i_{n,m}\Delta\tau_l, i_{n,m}\Delta f_{d,h}, \big(\tilde{\gamma}_{n,m}^2\big)^{(i)}\tilde{\boldsymbol{\Sigma}}^{(i)}\Big), \tag{27}$$

where

$$\big(\tilde{\gamma}_{n,m}^2\big)^{(i)} = \frac{1}{N}\boldsymbol{z}_{n,m}^{\dagger}\Big(\tilde{\boldsymbol{\Sigma}}^{(i)}\Big)^{-1}\boldsymbol{z}_{n,m}. \tag{28}$$

The average variation is defined as

$$\Delta\mathcal{L}(i) = \frac{1}{N_{\text{Trial}}}\sum_{n_T=1}^{N_{\text{Trial}}}\frac{\Big|\mathcal{L}_1^{(i,n_T)} - \mathcal{L}_1^{(i-1,n_T)}\Big|}{\Big|\mathcal{L}_1^{(i-1,n_T)}\Big|}, \tag{29}$$

where n_T indexes the Monte Carlo trial. In what follows, we average these values over 1000 Monte Carlo trials assuming that target position in the delay-Doppler domain randomly changes at each Monte Carlo trial.

Figure 2 plots the curves of $\Delta\mathcal{L}(i)$ versus i under the homogeneous environment for different SCNR, where the almost overlapping curves indicate that the value of SCNR has no significant impact on convergence performance. For the considered parameter settings, the $\Delta\mathcal{L}(i)$ decreases as i increases and is lower than 10^{-5} for $i \geq 9$.

The convergence performance under the heterogeneous environment is plotted in Figure 3, where for the considered parameter settings, $i = 15$ can ensure that the $\Delta\mathcal{L}(i)$ is lower than 10^{-5}.

Due to the uncertainty related to the characteristic of clutter and to find a good compromise between the computational burden and the optimisation performance, in what follows, we set $i_{\max} = 15$.

4.2 | Homogeneous Environment

Let us start with the CFAR analysis which concerns the sensitivity of the considered detectors with respect to the scaling factor and the covariance structure. To this end, we set the detection thresholds by assuming $P_{\text{fa}} = 10^{-3}$, CNR = 25 dB and $\rho = 0.9$, then we change these parameter values and estimate the corresponding $\widehat{P}_{\text{fa}}$ (under H_0).

Figure 4 shows that when the CNR changes, the $\widehat{P}_{\text{fa}}$ values returned by all the detectors are around the nominal $P_{\text{fa}} = 10^{-3}$, which indicates that the proposed detectors are almost insensitive to variations of the CNR at least for the considered range of parameter values.

Figure 5 highlights that detectors based upon the NSCM (i.e., the H-TS-GLRT-D, NSCM-TS-GLRT-D, H-C-TS-GLRT and NSCM-C-TS-GLRT) increase the false alarm rate when the clutter is highly correlated, namely when $\rho > 0.9$. On the other

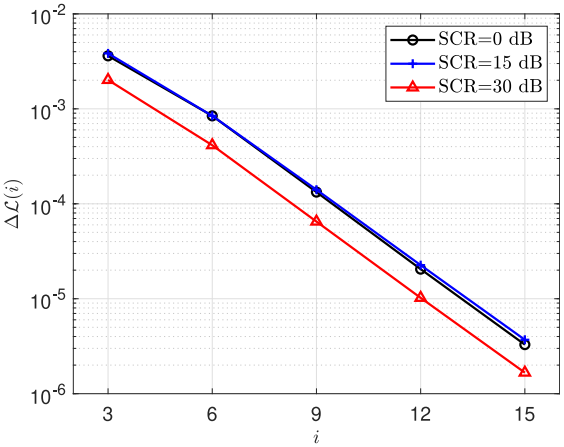

FIGURE 3 | $\Delta\mathcal{L}(i)$ versus i under H_1, $\nu = 0.5$, $\rho = 0.9$, heterogeneous environment.

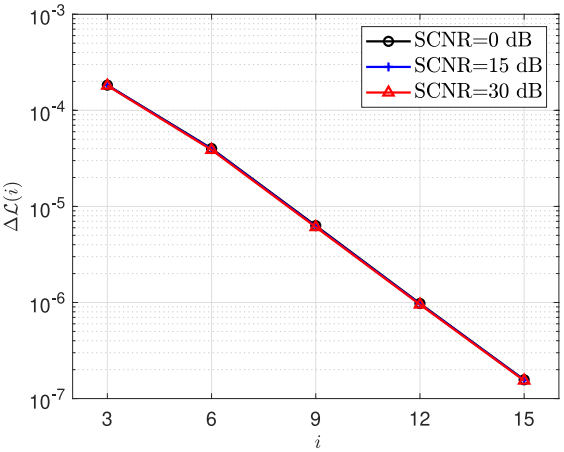

FIGURE 2 | $\Delta\mathcal{L}(i)$ versus i under H_1, CNR = 25 dB, $\rho = 0.9$, homogeneous environment.

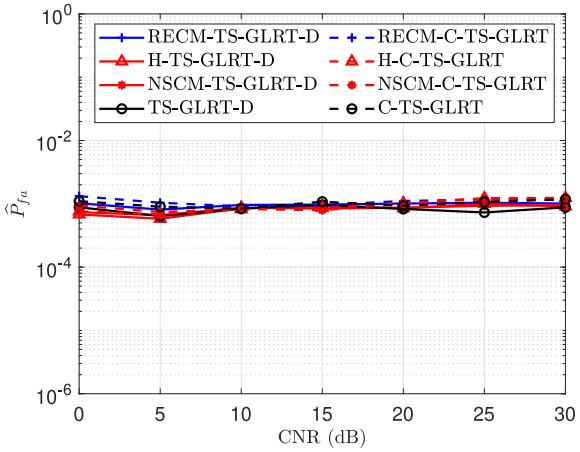

FIGURE 4 | $\widehat{P}_{\text{fa}}$ versus CNR with nominal $P_{\text{fa}} = 10^{-3}$, nominal CNR = 25 dB and nominal $\rho = 0.9$, homogeneous environment.

17518792, 2026, 1, Downloaded from https://ietresearch.onlinelibrary.wiley.com/doi/10.1049/rsn2.70127 by CochraneItalia, Wiley Online Library on [29/04/2026]. See the Terms and Conditions (https://onlinelibrary.wiley.com/terms-and-conditions) on Wiley Online Library for rules of use; OA articles are governed by the applicable Creative Commons License

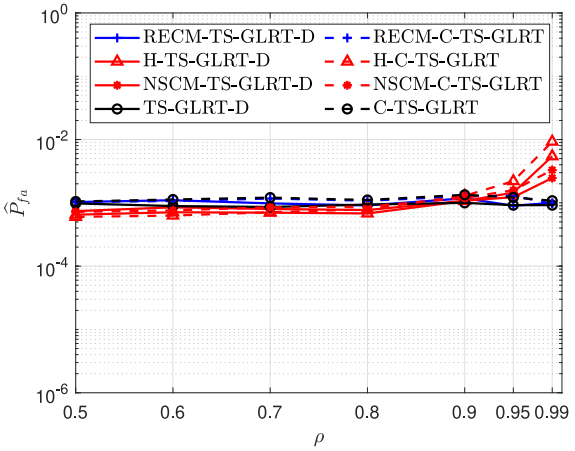

FIGURE 5 | $\widehat{P}_{\text{fa}}$ versus ρ with nominal $P_{\text{fa}} = 10^{-3}$, nominal CNR = 25 dB and nominal $\rho = 0.9$, homogeneous environment.

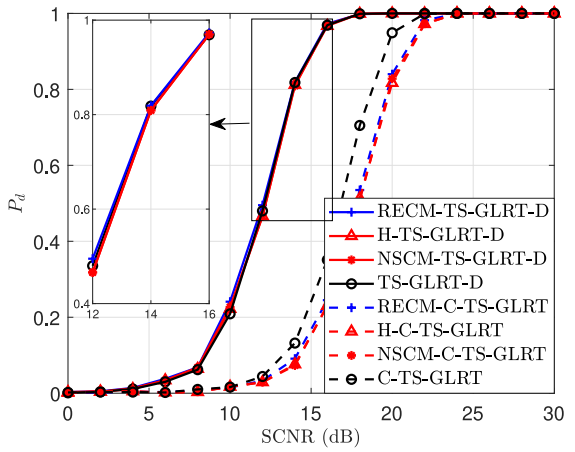

FIGURE 6 | P_{d} versus SCNR, CNR = 25 dB, $\rho = 0.9$, homogeneous environment.

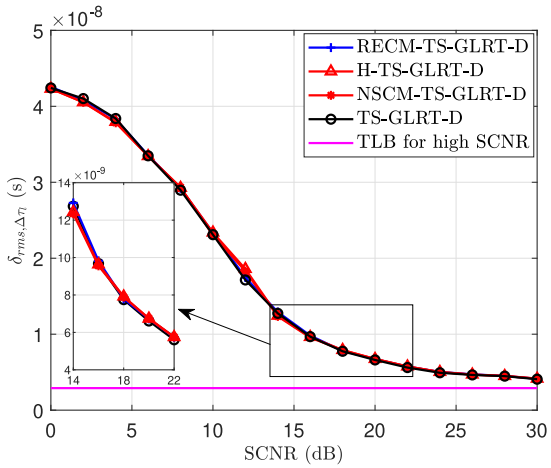

(a)

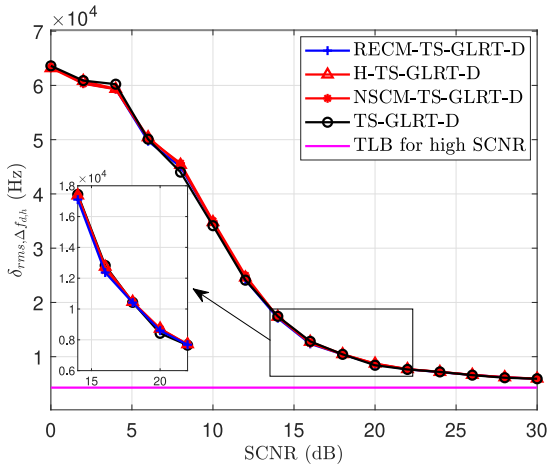

(b)

FIGURE 7 | RMS estimation errors for (a) $\Delta\tau_l$ and (b) $\Delta f_{d,h}$, CNR = 25 dB, $\rho = 0.9$, homogeneous environment.

hand, the other four detectors continue to provide a $\widehat{P}_{\text{fa}}$ that is very close to the nominal value.

The detection curves are shown in Figure 6 assuming CNR = 25 dB and $\rho = 0.9$ in a homogeneous environment. It turns out that the proposed detectors significantly outperform the considered counterparts due to the capitalisation of target energy spillover. Moreover, their performances are almost coincident and similar to that of the TS-GLRT-D.

Figure 7 contains the curves of RMS estimation errors of $\Delta\tau_l$ and $\Delta f_{d,h}$ versus SCNR of the proposed detectors as well as the TS-GLRT-D under homogeneous environment. The other competitors are not taken into account since they do not provide any estimate for the delay and Doppler differences. The plots show that the proposed detectors share similar estimation performance with the TS-GLRT-D. In particular, $\delta_{\text{rms},\Delta\tau_l}$ $\left(\delta_{\text{rms},\Delta f_{d,h}}\right)$ gradually approaches the Theoretical Lower-Bound (TLB) $\frac{\Delta\tau_s}{2N_\tau\sqrt{12}} \approx 2.9$ ns $\left(\frac{\Delta f_s}{2N_f * \sqrt{12}} \approx 4.3 \text{ kHz}\right)$ dictated by the grid resolution $\frac{\Delta\tau_s}{2N_\tau}$ $\left(\frac{\Delta f_s}{2N_f}\right)$.

The expressions of the decision statistics for each considered detector along with the respective execution times are reported in Table 1; the execution times are averaged over 1000 Monte Carlo trials in a homogeneous environment. As expected, the table shows that the three proposed detectors and the TS-GLRT-D are more time demanding than the traditional detectors. As a matter of fact, the former involves a 2-dimensional grid search to estimate the pair $(\Delta\tau_l, \Delta f_{d,h})$, thereby enabling location capabilities. Otherwise stated, the location capabilities are paid in terms of an increase of the computational cost. Notice that the H-TS-GLRT-D is the most time demanding among the proposed detectors, followed by the RECM-TS-GLRT-D and the NSCM-TS-GLRT-D. The TS-GLRT-D exhibits an execution time that is significantly lower than the other three because its decision statistic does not involve the scaling factor estimates.

4.3 | Heterogeneous Environment

Similar to the homogeneous environment, we still start with the CFAR analysis, where we use the detection thresholds estimated by assuming $P_{\text{fa}} = 10^{-3}$, $\nu = 0.5$ and $\rho = 0.9$, then we

17518792, 2026, 1, Downloaded from https://ietresearch.onlinelibrary.wiley.com/doi/10.1049/rsn2.70127 by CochraneItalia, Wiley Online Library on [29/04/2026]. See the Terms and Conditions (https://onlinelibrary.wiley.com/terms-and-conditions) on Wiley Online Library for rules of use; OA articles are governed by the applicable Creative Commons License

TABLE 1 | Average execution times over 1000 Monte Carlo trials, homogeneous environment.

Detector	Detection statistic	Time (ms)
RECM-TS-GLRT-D	$\max_{\Delta\tau_l,\Delta f_{d,h}} \frac{\left\lvert\sum_{(n,m)\in\Omega_t} \boldsymbol{p}^{\dagger}_{n-l,m-h}\left(\tilde{\gamma}^2_{n,m}\tilde{\boldsymbol{\Sigma}}^{(i\max)}\right)^{-1}\boldsymbol{z}_{n,m}\right\rvert^2}{\sum_{(n,m)\in\Omega_t} \boldsymbol{p}^{\dagger}_{n-l,m-h}\left(\tilde{\gamma}^2_{n,m}\tilde{\boldsymbol{\Sigma}}^{(i\max)}\right)^{-1}\boldsymbol{p}_{n-l,m-h}}$	118.9
H-TS-GLRT-D	$\max_{\Delta\tau_l,\Delta f_{d,h}} \frac{\left\lvert\sum_{(n,m)\in\Omega_t} \boldsymbol{p}^{\dagger}_{n-l,m-h}\left(\tilde{\gamma}^2_{n,m}\widehat{\boldsymbol{\Sigma}}\right)^{-1}\boldsymbol{z}_{n,m}\right\rvert^2}{\sum_{(n,m)\in\Omega_t} \boldsymbol{p}^{\dagger}_{n-l,m-h}\left(\tilde{\gamma}^2_{n,m}\widehat{\boldsymbol{\Sigma}}\right)^{-1}\boldsymbol{p}_{n-l,m-h}}$	120.7
NSCM-TS-GLRT-D	$\max_{\Delta\tau_l,\Delta f_{d,h}} \frac{\left\lvert\sum_{(n,m)\in\Omega_t} \boldsymbol{p}^{\dagger}_{n-l,m-h}\left(\widehat{\gamma}^2_{n,m}\widehat{\boldsymbol{\Sigma}}\right)^{-1}\boldsymbol{z}_{n,m}\right\rvert^2}{\sum_{(n,m)\in\Omega_t} \boldsymbol{p}^{\dagger}_{n-l,m-h}\left(\widehat{\gamma}^2_{n,m}\widehat{\boldsymbol{\Sigma}}\right)^{-1}\boldsymbol{p}_{n-l,m-h}}$	76.6
TS-GLRT-D	$\max_{\Delta\tau_l,\Delta f_{d,h}} \frac{\left\lvert\sum_{(n,m)\in\Omega_t} \boldsymbol{p}^{\dagger}_{n-l,m-h}\widehat{\boldsymbol{M}}^{-1}\boldsymbol{z}_{n,m}\right\rvert^2}{\sum_{(n,m)\in\Omega_t} \boldsymbol{p}^{\dagger}_{n-l,m-h}\widehat{\boldsymbol{M}}^{-1}\boldsymbol{p}_{n-l,m-h}}$	7.4
RECM-C-TS-GLRT	$\sum_{(n,m)\in\Omega_{l,h}} \frac{\left\lvert\boldsymbol{p}^{\dagger}\left(\tilde{\gamma}^2_{n,m}\tilde{\boldsymbol{\Sigma}}^{(i\max)}\right)^{-1}\boldsymbol{z}_{n,m}\right\rvert^2}{\boldsymbol{p}^{\dagger}\left(\tilde{\gamma}^2_{n,m}\tilde{\boldsymbol{\Sigma}}^{(i\max)}\right)^{-1}\boldsymbol{p}}$	46.4
H-C-TS-GLRT	$\sum_{(n,m)\in\Omega_{l,h}} \frac{\left\lvert\boldsymbol{p}^{\dagger}\left(\tilde{\gamma}^2_{n,m}\widehat{\boldsymbol{\Sigma}}\right)^{-1}\boldsymbol{z}_{n,m}\right\rvert^2}{\boldsymbol{p}^{\dagger}\left(\tilde{\gamma}^2_{n,m}\widehat{\boldsymbol{\Sigma}}\right)^{-1}\boldsymbol{p}}$	48.2
NSCM-C-TS-GLRT	$\sum_{(n,m)\in\Omega_{l,h}} \frac{\left\lvert\boldsymbol{p}^{\dagger}\left(\widehat{\gamma}^2_{n,m}\widehat{\boldsymbol{\Sigma}}\right)^{-1}\boldsymbol{z}_{n,m}\right\rvert^2}{\boldsymbol{p}^{\dagger}\left(\widehat{\gamma}^2_{n,m}\widehat{\boldsymbol{\Sigma}}\right)^{-1}\boldsymbol{p}}$	3.6
C-TS-GLRT	$\sum_{(n,m)\in\Omega_{l,h}} \frac{\left\lvert\boldsymbol{p}^{\dagger}\widehat{\boldsymbol{M}}^{-1}\boldsymbol{z}_{n,m}\right\rvert^2}{\boldsymbol{p}^{\dagger}\widehat{\boldsymbol{M}}^{-1}\boldsymbol{p}}$	0.2

change the parameter settings and estimate the actual $\widehat{P}_{\text{fa}}$ to study the sensitivity of the detectors with respect to ν and ρ.

As expected, in Figure 8, the curves of the $\widehat{P}_{\text{fa}}$ associated with the TS-GLRT-D and C-TS-GLRT significantly deviate from the nominal behaviour. As a consequence, when data are heterogeneous, these detectors cannot maintain a constant false alarm rate at least for the considered range of values for ν. On the contrary, the $\widehat{P}_{\text{fa}}$ values returned by the other detectors are closely displaced around the nominal $P_{\text{fa}} = 10^{-3}$ regardless the values of ν.

Figure 9 confirms what observed in the homogeneous environment, where the H-TS-GLRT-D, NSCM-TS-GLRT-D, H-C-TS-GLRT and NSCM-C-TS-GLRT cannot maintain $\widehat{P}_{\text{fa}}$ values close to the nominal P_{fa} for $\rho > 0.9$.

Figure 10 focuses on the detection performance under heterogeneous environment. From the comparison with Figure 6, it turns out that when the background is non-homogeneous, the TS-GLRT-D and the C-TS-GLRT experience a significant detection loss with respect to the homogeneous environment, whereas the other detectors still provide a good detection performance; the proposed detectors significantly outperform their corresponding competitors. More importantly, the prominent advantages of the proposed detectors with respect to the TS-GLRT-D demonstrate the effectiveness of the RECM in dealing with compound Gaussian background.

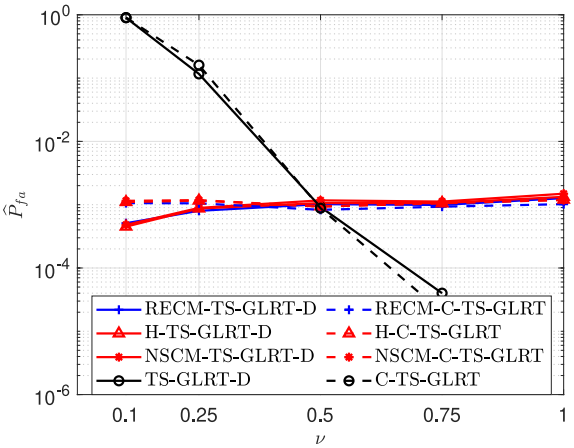

FIGURE 8 | $\widehat{P}_{\text{fa}}$ versus ν with nominal $P_{\text{fa}} = 10^{-3}$, nominal $\nu = 0.5$ and nominal $\rho = 0.9$, heterogeneous environment.

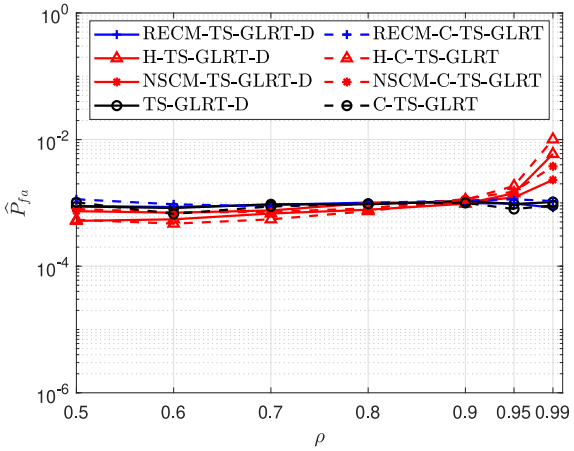

FIGURE 9 | $\widehat{P}_{\text{fa}}$ versus ρ with nominal $P_{\text{fa}} = 10^{-3}$, nominal $\nu = 0.5$ and nominal $\rho = 0.9$, heterogeneous environment.

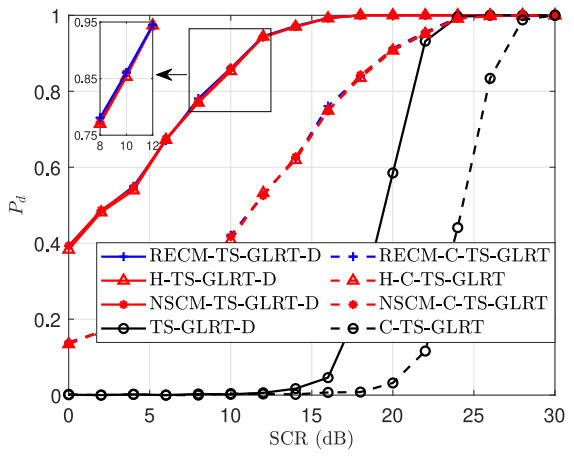

FIGURE 10 | P_{d} versus SCR, $\nu = 0.5$, $\rho = 0.9$, heterogeneous environment.

The RMS estimation error curves are shown in Figure 11 as functions of the SCR under heterogeneous environment. Also in this case, a performance degradation occurs for the TS-GLRT-D

17518792, 2026, 1, Downloaded from https://ietresearch.onlinelibrary.wiley.com/doi/10.1049/rsn2.70127 by CochraneItalia, Wiley Online Library on [29/04/2026]. See the Terms and Conditions (https://onlinelibrary.wiley.com/terms-and-conditions) on Wiley Online Library for rules of use; OA articles are governed by the applicable Creative Commons License

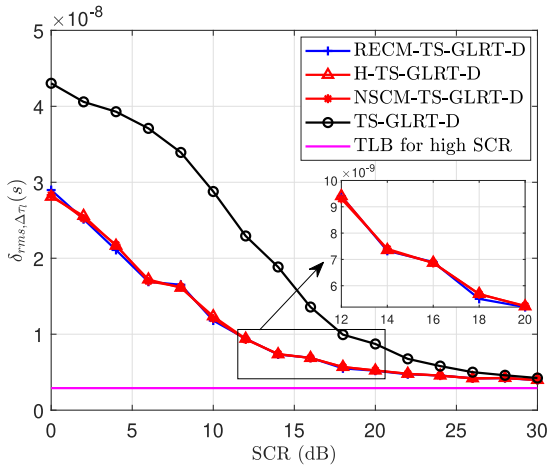

(a)

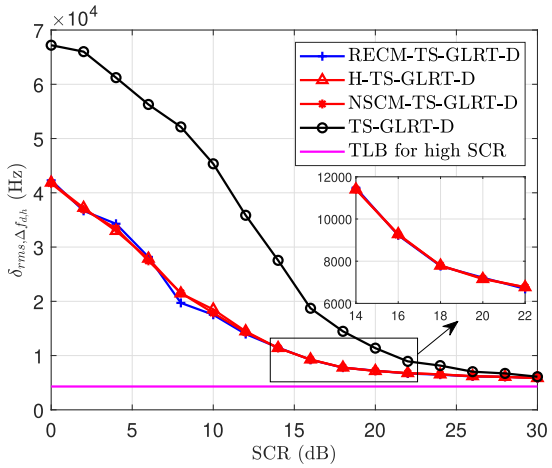

(b)

FIGURE 11 | RMS estimation errors of (a) $\Delta\tau_l$ and (b) $\Delta f_{d,h}$, $\nu = 0.5$, $\rho = 0.9$, heterogeneous environment.

with respect to the homogeneous environment, and the proposed detectors exhibit significant performance advantages.

Summarising, the analysis has singled out the RECM-TS-GLRT-D as the detector that can operate in both homogeneous and heterogeneous scenarios providing excellent detection performance whilst maintaining an almost constant false alarm rate but at the price of an increase of the computational load.

5 | Conclusion

In this paper, three MIMO radar detection algorithms, capable of jointly detecting a point-like target and estimating its position in the delay-Doppler domain, have been designed for heterogeneous environments. Specifically, we have extended the binary hypothesis test formulated in [20] from homogeneous environments to heterogeneous environments and derived detectors resorting to the two-step GLRT design criterion. Instead of the SCM used in homogeneous environments, the NSCM and the RECM have been utilised for background parameter estimation. In addition to deciding for the presence or absence of a target, the proposed algorithms can provide estimates of the target position in the delay-Doppler domain as a by-product. At the analysis stage, we have compared the newly proposed detectors with the TS-GLRT-D designed for homogeneous environments in [20], as well as the corresponding classical decision schemes for MIMO radars and extended targets. Numerical examples have shown that in terms of detection and estimation performance, the newly proposed detectors significantly outperform the competitors in heterogeneous environments whilst possessing satisfying performance. In addition, the analysis of CFAR behaviour has demonstrated that regardless of the environment nature, the H-TS-GLRT-D and the NSCM-TS-GLRT-D are insensitive to changes in scaling factor and the RECM-TS-GLRT-D remains insensitive to both changes in scaling factor and covariance structure for the clutter component.

Future research directions might investigate scenarios involving multiple dominant scatterers in contiguous delay-Doppler bins. It would also be important to compare the detection performance and the CFAR behaviour of detectors based upon different design criteria such as those addressed in [38]. Finally, it is worth investigating the effects on the performance of the ambiguity function mismatch or the incorporation of structured interference covariance matrices into the detector design. These advancements would better address realistic target models and complex clutter scenarios.

Author Contributions

Tianqi Wang: methodology, validation, writing – review and editing. **Chaoran Yin:** investigation, methodology. **Da Xu:** methodology, validation, writing – review and editing. **Chengpeng Hao:** methodology, validation, writing – review and editing. **Danilo Orlando:** writing – review and editing. **Giuseppe Ricci:** conceptualization, methodology.

Acknowledgements

The work of Danilo Orlando was partially supported by the Italian Ministry of Education and Research (MUR) in the framework of the FoReLab project (Departments of Excellence).

Funding

The authors have nothing to report.

Conflicts of Interest

The authors declare no conflicts of interest.

Data Availability Statement

Research data are not shared.

References

1. W. L. Melvin and J. Scheer, *Principles of Modern Radar: Advanced Techniques, Radar, Sonar and Navigation* (Institution of Engineering and Technology, 2012).

2. J. Li and P. Stoica, *MIMO Radar Signal Processing* (John Wiley & Sons, 2008).

3. J. Li and P. Stoica, "MIMO Radar With Colocated Antennas," *IEEE Signal Processing Magazine* 24, no. 5 (2007): 106–114, https://doi.org/10.1109/msp.2007.904812.

17518792, 2026, 1, Downloaded from https://ietresearch.onlinelibrary.wiley.com/doi/10.1049/rsn2.70127 by CochraneItalia, Wiley Online Library on [29/04/2026]. See the Terms and Conditions (https://onlinelibrary.wiley.com/terms-and-conditions) on Wiley Online Library for rules of use; OA articles are governed by the applicable Creative Commons License

4. L. Xu, J. Li and P. Stoica, "Target Detection and Parameter Estimation for MIMO Radar Systems," *IEEE Transactions on Aerospace and Electronic Systems* 44, no. 3 (2008): 927–939, https://doi.org/10.1109/taes.2008.4655353.

5. H. Xu, J. Wang, J. Yuan and X. Shan, "Colocated MIMO Radar Transmit Beamspace Design for Randomly Present Target Detection," *IEEE Signal Processing Letters* 22, no. 7 (2015): 828–832, https://doi.org/10.1109/lsp.2014.2371241.

6. W. Liu, Y. Wang, J. Liu, W. Xie, H. Chen and W. Gu, "Adaptive Detection Without Training Data in Colocated MIMO Radar," *IEEE Transactions on Aerospace and Electronic Systems* 51, no. 3 (2015): 2469–2479, https://doi.org/10.1109/taes.2015.130754.

7. J. Liu, S. Zhou, W. Liu, J. Zheng, H. Liu and J. Li, "Tunable Adaptive Detection in Colocated MIMO Radar," *IEEE Transactions on Signal Processing* 66, no. 4 (2018): 1080–1092, https://doi.org/10.1109/tsp.2017.2778693.

8. J. Liu, W. Liu, J. Han, B. Tang, Y. Zhao and H. Yang, "Persymmetric GLRT Detection in MIMO Radar," *IEEE Transactions on Vehicular Technology* 67, no. 12 (2018): 11913–11923, https://doi.org/10.1109/tvt.2018.2877265.

9. B. Tang and P. Stoica, "MIMO Multifunction RF Systems: Detection Performance and Waveform Design," *IEEE Transactions on Signal Processing* 70 (2022): 4381–4394, https://doi.org/10.1109/tsp.2022.3202315.

10. W. Zhai, X. Wang, X. Cao, M. S. Greco and F. Gini, "Reinforcement Learning Based Dual-Functional Massive MIMO Systems for Multi-Target Detection and Communications," *IEEE Transactions on Signal Processing* 71 (2023): 741–755, https://doi.org/10.1109/tsp.2023.3252885.

11. S. Yang, W. Yi, A. Jakobsson, Y. Wang and H. Xiao, "Weak Signal Detection With Low-Bit Quantization in Colocated MIMO Radar," *IEEE Transactions on Signal Processing* 71 (2023): 447–460, https://doi.org/10.1109/tsp.2023.3246233.

12. B. Friedlander, "On Signal Models for MIMO Radar," *IEEE Transactions on Aerospace and Electronic Systems* 48, no. 4 (2012): 3655–3660, https://doi.org/10.1109/taes.2012.6324753.

13. B. Friedlander, "On Spatial Processing in MIMO Radar," in *2011 Conference Record of the Forty Fifth Asilomar Conference on Signals, Systems and Computers (ASILOMAR)*, (2011), 2075–2079.

14. M. A. Richards, J. A. Scheer and W. A. Holm, *Principles of Modern Radar: Basic Principles* (Scitech Publishing, 2010).

15. D. Orlando and G. Ricci, "Adaptive Radar Detection and Localization of a Point-Like Target," *IEEE Transactions on Signal Processing* 59, no. 9 (2011): 4086–4096, https://doi.org/10.1109/tsp.2011.2159602.

16. C. Hao, S. Gazor, G. Foglia, B. Liu and C. Hou, "Persymmetric Adaptive Detection and Range Estimation of a Small Target," *IEEE Transactions on Aerospace and Electronic Systems* 51, no. 4 (2015): 2590–2604, https://doi.org/10.1109/taes.2015.140517.

17. A. Aubry, A. De Maio, G. Foglia, C. Hao and D. Orlando, "Radar Detection and Range Estimation Using Oversampled Data," *IEEE Transactions on Aerospace and Electronic Systems* 51, no. 2 (2015): 1039–1052, https://doi.org/10.1109/taes.2014.130364.

18. L. Yan, C. Hao, D. Orlando, A. Farina and C. Hou, "Parametric Space-Time Detection and Range Estimation of Point-Like Targets in Partially Homogeneous Environment," *IEEE Transactions on Aerospace and Electronic Systems* 56, no. 2 (2020): 1228–1242, https://doi.org/10.1109/taes.2019.2928672.

19. C. Hao, D. Orlando, J. Liu and C. Yin, *Advances in Adaptive Radar Detection and Range Estimation* (Springer Nature Singapore, 2021).

20. T. Wang, C. Yin, D. Xu, C. Hao, D. Orlando and G. Ricci, "Joint Detection and Delay-Doppler Estimation Algorithms for Mimo Radars," *IEEE Transactions on Signal Processing* 72 (2024): 809–823, https://doi.org/10.1109/tsp.2024.3355753.

21. E. J. Kelly, "An Adaptive Detection Algorithm," *IEEE Transactions on Aerospace and Electronic Systems*, no. 2 (1986): 115–127, https://doi.org/10.1109/taes.1986.310745.

22. F. C. Robey, D. R. Fuhrmann, E. J. Kelly and R. Nitzberg, "A CFAR Adaptive Matched Filter Detector," *IEEE Transactions on Aerospace and Electronic Systems* 28, no. 1 (1992): 208–216, https://doi.org/10.1109/7.135446.

23. T. Wang, C. Yin, D. Xu, C. Hao, D. Orlando and G. Ricci, "Analysis of MIMO Radar Detection Algorithms With Location Capabilities: CFAR Property and Selectivity," *IEEE Transactions on Aerospace and Electronic Systems* 61, no. 2 (2025): 5426–5435, https://doi.org/10.1109/taes.2024.3488688.

24. T. Wang, C. Yin, D. Xu, C. Hao, D. Orlando and G. Ricci, "Performance Analysis of a Joint Detection and Delay-Doppler Estimation Algorithm for MIMO Radars," in *2024 International Radar Conference (RADAR)*, 2024), 1–6.

25. K. Ward, "Erratum: Compound Representation of High Resolution Sea Clutter," *Electronics Letters* 17, no. 22 (1981): 862, https://doi.org/10.1049/el:19810599.

26. K. D. Ward, C. J. Baker and S. Watts, "Maritime Surveillance Radar. Part 1: Radar Scattering From the Ocean Surface," *IEE Proceedings F (Radar and Signal Processing)* 137, no. 2 (1990): 51–62, https://doi.org/10.1049/ip-f-2.1990.0009.

27. M. Greco, F. Gini and M. Rangaswamy, "Statistical Analysis of Measured Polarimetric Clutter Data at Different Range Resolutions, Radar, Sonar and Navigation," *IEE Proceedings* 153, no. 6 (2006): 473–481, https://doi.org/10.1049/ip-rsn:20060045.

28. E. Conte and M. Longo, "Characterisation of Radar Clutter as a Spherically Invariant Random Process," *IEE Proceedings, F. Communications, radar and signal processing* 134, no. 2 (1987): 191–197, https://doi.org/10.1049/ip-f-1.1987.0035.

29. E. Conte, M. Longo and M. Lops, "Modelling and Simulation of Non-Rayleigh Radar Clutter, Radar and Signal Processing," *IEE Proceedings F (Radar and Signal Processing)* 138, no. 2 (1991): 121–130, https://doi.org/10.1049/ip-f-2.1991.0018.

30. A. Coluccia, D. Orlando and G. Ricci, "A GLRT-Like CFAR Detector for Heterogeneous Environments," *Signal Processing* 194 (2022): 108401, https://doi.org/10.1016/j.sigpro.2021.108401.

31. E. Conte, M. Lops and G. Ricci, "Asymptotically Optimum Radar Detection in Compound-Gaussian Clutter," *IEEE Transactions on Aerospace and Electronic Systems* 31, no. 2 (1995): 617–625, https://doi.org/10.1109/7.381910.

32. J. Liu, D. Massaro, D. Orlando and A. Farina, "Radar Adaptive Detection Architectures for Heterogeneous Environments," *IEEE Transactions on Signal Processing* 68 (2020): 4307–4319, https://doi.org/10.1109/tsp.2020.3009836.

33. E. Conte, M. Lops and G. Ricci, "Adaptive Detection Schemes in Compound-Gaussian Clutter," *IEEE Transactions on Aerospace and Electronic Systems* 34, no. 4 (1998): 1058–1069, https://doi.org/10.1109/7.722671.

34. E. Conte, A. De Maio and G. Ricci, "Recursive Estimation of the Covariance Matrix of a Compound-Gaussian Process and Its Application to Adaptive CFAR Detection," *IEEE Transactions on Signal Processing* 50, no. 8 (2002): 1908–1915, https://doi.org/10.1109/tsp.2002.800412.

35. B. Friedlander, "On Signal Models for MIMO Radar," *IEEE Transactions on Aerospace and Electronic Systems* 48, no. 4 (2012): 3655–3660, https://doi.org/10.1109/taes.2012.6324753.

36. E. Conte, M. Lops and G. Ricci, "Adaptive Radar Detection in Compound-Gaussian Clutter," *Proceedings of the Seventh European Signal Processing Conference (EUSIPCO-94)* Vol, 94 (1994), 526–529.

37. E. Conte, A. De Maio and G. Ricci, "GLRT-Based Adaptive Detection Algorithms for Range-Spread Targets," *IEEE Transactions on Signal*

17518792, 2026, 1, Downloaded from https://ietresearch.onlinelibrary.wiley.com/doi/10.1049/rsn2.70127 by CochraneItalia, Wiley Online Library on [29/04/2026]. See the Terms and Conditions (https://onlinelibrary.wiley.com/terms-and-conditions) on Wiley Online Library for rules of use; OA articles are governed by the applicable Creative Commons License

Processing 49, no. 7 (2001): 1336–1348, https://doi.org/10.1109/78.928688.

38. D. Ciuonzo, A. De Maio and D. Orlando, "A Unifying Framework for Adaptive Radar Detection in Homogeneous Plus Structured Interference—Part II: Detectors Design," *IEEE Transactions on Signal Processing* 64, no. 11 (2016): 2907–2919, https://doi.org/10.1109/tsp.2016.2519005.

Appendix A

In this appendix, we provide the proofs of Equations (11) and (12). Let us start from the former and observe that the objective function in Equation (10) is radially unbounded with respect to the real and imaginary parts of α_t denoted by $\alpha_{t,r} \in \mathbb{R}$ and $\alpha_{t,i} \in \mathbb{R}$, respectively. As a consequence, we can search the minimum within its domain by setting to zero its first complex derivative with respect to α_t^*. To this end, we use the following definition

$$\frac{\partial f(\alpha_t)}{\partial \alpha_t^*} = \frac{1}{2}\left[\frac{\partial f(\alpha_t)}{\alpha_{t,r}} + j\frac{\partial f(\alpha_t)}{\alpha_{t,i}}\right]. \tag{A1}$$

Thus, the derivative of the objective function in Equation (10) has the following expression

$$\alpha_t \sum_{(n,m)\in\Omega_t} \boldsymbol{p}_{n-l,m-h}^{\dagger}\boldsymbol{M}_{n,m}^{-1}\boldsymbol{p}_{n-l,m-h} - \sum_{(n,m)\in\Omega_t} \boldsymbol{p}_{n-l,m-h}^{\dagger}\boldsymbol{M}_{n,m}^{-1}\boldsymbol{z}_{n,m} \tag{A2}$$

and setting the above quantity to zero we obtain Equation (11).

As for Equation (12), let us consider the numerator and the denominator of the left-hand side of Equation (7) and notice that, neglecting the same constants, their logarithms can be written as

$$\begin{aligned} &-\sum_{(n,m)\in\Omega_t} \left(\boldsymbol{z}_{n,m} - \alpha_t \boldsymbol{p}_{n-l,m-h}\right)^{\dagger} \boldsymbol{M}_{n,m}^{-1}\left(\boldsymbol{z}_{n,m} - \alpha_t \boldsymbol{p}_{n-l,m-h}\right) \\ &\qquad - \sum_{(n,m)\in\Omega_{l,h}\setminus\Omega_t} \boldsymbol{z}_{n,m}^{\dagger}\boldsymbol{M}_{n,m}^{-1}\boldsymbol{z}_{n,m} \end{aligned} \tag{A3}$$

and

$$-\sum_{(n,m)\in\Omega_{l,h}} \boldsymbol{z}_{n,m}^{\dagger}\boldsymbol{M}_{n,m}^{-1}\boldsymbol{z}_{n,m},$$

respectively.

Now, replacing α_t with Equation (11) into the 'logarithm of the numerator', we obtain

$$-\sum_{(n,m)\in\Omega_{l,h}} \boldsymbol{z}_{n,m}^{\dagger}\boldsymbol{M}_{n,m}^{-1}\boldsymbol{z}_{n,m} + \frac{\left|\sum_{(n,m)\in\Omega_t} \boldsymbol{p}_{n-l,m-h}^{\dagger}\boldsymbol{M}_{n,m}^{-1}\boldsymbol{z}_{n,m}\right|^2}{\sum_{(n,m)\in\Omega_t} \boldsymbol{p}_{n-l,m-h}^{\dagger}\boldsymbol{M}_{n,m}^{-1}\boldsymbol{p}_{n-l,m-h}}. \tag{A4}$$

Finally, the difference of the two logarithms returns Equation (12).

17518792, 2026, 1, Downloaded from https://ietresearch.onlinelibrary.wiley.com/doi/10.1049/rsn2.70127 by CochraneItalia, Wiley Online Library on [29/04/2026]. See the Terms and Conditions (https://onlinelibrary.wiley.com/terms-and-conditions) on Wiley Online Library for rules of use; OA articles are governed by the applicable Creative Commons License